Atmos. Chem. Phys. Discuss., 5, 3269–3312, 2005
www.atmos-chem-phys.org/acpd/5/3269/
SRef-ID: 1680-7375/acpd/2005-5-3269
European Geosciences Union

Atmospheric Chemistry and Physics Discussions

The structure of the haze plume over the Indian Ocean during INDOEX: tracer simulations and LIDAR observations

G. Forêt[1], C. Flamant[2], S. Cautenet[1], J. Pelon[2], F. Minvielle[1], M. Taghavi[1], and P. Chazette[3]

[1]Laboratoire de Météorologie Physique, Université Blaise Pascal, Aubière, France
[2]Institut Pierre-Simon Laplace/Service d'Aéronomie, Université Pierre et Marie Curie, Paris, France
[3]Institut Pierre-Simon Laplace/Laboratoire des Sciences du Climat et de l'Environnement, Centre de l'Energie Atomique, Saclay, France

Received: 4 January 2005 – Accepted: 18 February 2005 – Published: 24 May 2005

Correspondence to: G. Forêt (foret@lisa.univ-paris12.fr)

© 2005 Author(s). This work is licensed under a Creative Commons License.

Abstract

Three-dimensional nested tracer simulations of a pollution plume originating from the Indian sub-continent over the Indian Ocean in the framework of the Indian Ocean Experiment (INDOEX) between 5 and 9 March 1999 were performed with the Regional Atmospheric Modeling System (RAMS) to provide insight into the transport patterns of the pollutants as well as investigate the dynamical mechanisms controlling the vertical structure of the plume and its evolution in the vicinity of the Maldives Islands. Airborne and ground-based LIDAR observations of the structure of the haze plume made on 7 March 1999 were used to assess the quality of the simulations as well as the impact of grid resolution on the vertical structure of the simulated plume. It is shown that, over the Arabian Sea, in the vicinity of the Maldives Islands, the pollutants composing the plume observed by the airborne LIDAR essentially originated from the city of Madras and that the vertical structure of the plume was controlled by the diurnal cycle of the continental boundary layer depth. A combination of tracer simulations and remote sensing observations (airborne LIDAR, ship-borne photometer, ground-based LIDAR in Goa) was used to analyse the diurnal evolution of the haze plume over the sea. We find evidence that the sea breeze circulation and orographic lifting taking place in the southern part of the Indian sub-continent during the day time play a crucial role in the modulation of the continental boundary layer depth, and in turn, the haze plume depth. The dynamical processes, as well as entrainment at the top of the marine atmospheric boundary layer, also play a crucial role in re-circulating a fraction of the tracers transported over ocean by the monsoon flow above the marine atmospheric boundary layer in the landward (southwesterly) branch of breeze circulation during the next day. This in turn leads to pollutant accumulation in the vicinity of the Indian coastline. Nevertheless, this contribution to the total aerosol load observed during the INDOEX intensive field phase is shown to small compared to that related to massive advection of aerosol from the continent. The nesting of a high horizontal resolution domain (5 km, with 39 vertical levels below 4000 m above mean seal level), allows a better representation of

ACPD

5, 3269–3312, 2005

local dynamics, sea and mountains breezes circulations, and therefore a noticeable improvement in the representation of the pollutants plume in the simulation.

1. Introduction

Due to their radiative impact on the Earth's energy budget and the substantial increase of their global mean burden from pre-industrial times to the present-day, aerosols have become important actors of climate change. Except in remote oceanic locations, the atmospheric aerosol burden is generally composed of a wide variety of natural aerosols (e.g. mineral dust, sea salts) and anthropogenic aerosols (e.g. sulfate and carbonaceous aerosols). All aerosols have the ability to intercept short and long wave radiation and reflect back incident solar radiation into space (direct effect). Some aerosols act as cloud condensation nuclei and thereby determine the cloud droplet number concentration and efficiency. They modify cloud optical properties by increasing cloud albedo (first indirect effect) or cloud lifetime and precipitation (second indirect effect). Both effects result in a cooling, which partially offsets the greenhouse gas warming. Aerosols absorbing solar radiation may be conducive to warming in the lower atmosphere and induce (locally) a reduction of the cloud cover (semi-direct effect).

The magnitude of all these competing effects is difficult to assess because of (i) the highly variable three-dimensional distribution of aerosols with time due to fluctuations in source strength and location; (ii) the paramount diversity of aerosols with highly variable physico-chemical properties which interact differently with hydrological cycle. For instance, using a global circulation model, Lohmann and Feichter (2001) compared the magnitude of all these competing effects and found that, even though the indirect effects dominated globally, the semi-direct effect could be important locally.

Several experiments such as the Transport of Aerosols and Radiative Forcing Experiment (TARFOX) (Russell et al., 1999), the second Aerosol Characterization Experiment (ACE-2) (Raes et al., 2000), the Indian Ocean Experiment (INDOEX) (Ramanathan et al., 2001) and the Asian Aerosol Characterization Experiment (ACE-Asia) (Huebert et

ACPD
5, 3269–3312, 2005

al., 2003) have been conducted to reduce the uncertainties associated with the diverse aerosol effects. In the framework of these experiments, an impressive amount of ground-based, ship-borne and airborne in situ as well as remote sensing instruments have been deployed to better understand and characterize the aerosol optical and radiative properties in the regions of interest. Such experiments also aimed at improving the quality of satellite aerosol retrievals and contribute to the assessment of aerosol radiative forcing at the regional scale.

In such integrated analyses, models are valuable tools to bridge the gap between in situ and satellite measurements. They offer large spatial and temporal coverage which provides opportunities to study the formation of pollution plumes, the transport patterns of aerosols as well as their radiative impact based on their composition. Nevertheless, such modeling studies are still not fully reliable due to uncertainties associated with the characterization of aerosol sources and emissions. Poor knowledge of the evolution undergone by aerosols during long-term transport is another source of uncertainty. Finally, as such studies are generally undertaken in the vicinity of coastal areas (to this day, aerosol radiative forcing cannot be assessed over continents), the complex dynamics occurring in these regions (including the diurnal cycle of convection over land) needs to be well simulated. This is crucial as the knowledge of the vertical distribution of aerosols within a pollution plume is key to properly assessing the associated radiative forcing.

Only a few instruments can provide information on the vertical distribution of aerosols, for instance laser remote sensing systems (i.e. LIDARs). During INDOEX for example, an impressive amount of details concerning the structure of the plume associated with pollution outbreaks over the continent as well as its evolution during the transport over the ocean has been provided by ground-based (Léon et al., 2001; Chazette, 2003; Franke et al., 2003), ship-borne (Welton et al., 2002) and airborne (Pelon et al., 2002) LIDARs.

In this paper, we analyse the three-dimensional (3-D) structure of the Indo-Asian pollution plume transported from the Indian sub-continent in early March of 1999 over

the Indian Ocean using a combination of mesoscale simulations (made with the model Regional Atmospheric Modeling System -RAMS) and LIDAR measurements. LIDAR observations were acquired in the course of the INDOEX Intensive Field Phase (IFP), held during the 1999 winter monsoon period. We focus our study on LIDAR measurements made on 7 March 1999 during a Mystère-20 (M-20) mission north of the Maldives Islands (Pelon et al., 2002). The region investigated is shown in Fig. 1.

The focus of this paper is to validate, in a first step, the high resolution simulations of 3-D structure of the plume obtained with the RAMS over the Indian Ocean in the vicinity of the Maldives Islands using LIDAR measurements. At this point we have only considered passive tracers as a proxy for anthropogenic aerosols. We also have not considered the entire Indian sub-continent as a source region, but rather have selected 4 cities (Bombay, Madras, Hyderabad and Calcutta) as the major emission sources. This exercise is nearly impossible to do based on realistic emissions of "real aerosols" because sources are numerous and aerosols cannot be tagged to their sources. Our objective is to determine the origin of the aerosol composing the plume observed by LIDAR on 7 March 1999 (Pelon et al., 2002) and to assess whether the transport patterns leading to the simulated vertical structure of the plume are consistent with observations.

In Sect. 2, we present briefly the INDOEX experiment, the synoptic conditions during the first week of March 1999 as well as the observations made on 7 March 1999, during the IFP. In Sect. 3, the RAMS model and the simulation designed for INDOEX are presented. In Sect. 4, using the tracer simulations, we discuss the origin of the aerosol composing the plume near the Maldives Islands and the vertical structure of the plume. We also discuss the diurnal evolution of the structure of the monsoon plume as well as its propagation over the Indian Ocean, in the light of simulations as well as ship-borne and ground-based remote sensing observations. Finally, we discuss the sensitivity of the plume structure to the grid resolution as well as the vertical structure of the plume simulated with RAMS. In Sect. 5, we summarize and conclude.

ACPD
5, 3269–3312, 2005

2. The Indian Ocean experiment

2.1. Background

The INDOEX IFP (February–March 1999) highlighted the formation of an important pollutant haze over India, Bay of Bengal and Arabian Sea, spreading as far south as the Intertropical Convergence Zone (ITCZ) (Lelieveld et al., 2001) during the winter monsoon. The main mechanisms responsible of the formation of this huge plume have been described in Ramanathan et al. (2001) and Verver et al. (2001) and are only briefly recalled here.

India is known as an important source region of anthropogenic aerosols (Lelieveld et al., 2001). Gaseous pollution emissions in India are essentially related to domestic biofuel and agricultural waste burning (Streets and Waldhoff, 1999; Sinha et al., 1998; Mahapatra and Michel, 1999). Sources are located in the large cities of India, as well as throughout the country. During the second half of the INDOEX IFP (mid Febuary to late March), a high pressure area was located over the north-western part of the Indian continent and a low pressure system was over western Indonesia (Rasch et al., 2001). A study of tagged radon transport (Rasch et al., 2001) demonstrated that, in the region of interest for this study – i.e. the part of the Indian Ocean between the Maldives and the Indian sub-continent (delimited by the smallest box in Fig. 1), synoptic conditions favored long-range transport of pollutants from India exclusively for the beginning of March.

The dry monsoon initiated the buildup of the haze over the Indian sub-continent as shown by the seasonal cycle of the Aerosol Optical Depth (AOD) and aerosol burden over the western coast of India observed at Goa and Dharwad (Léon et al., 2001). During this period, the highly polluted air masses are generally observed to be transported over the Indian Ocean by the northerly/northeasterly winter monsoon flow. Under such meteorological conditions pollutants may undergo long range transport. During the INDOEX IFP, ground-based, ship borne and airborne measurements revealed very high concentrations of aerosols and trace gases over the Arabian sea, the pollution levels

sometimes reaching those observed in North America suburbs (Lelieveld et al., 2001). The Maldives Islands are generally observed to be the focus point of air mass from different origins in the Marine Atmospheric Boundary Layer (MABL) and aloft during the winter monsoon (e.g. Reiner et al., 2001; Pelon et al., 2002). Meteosat 5 exhibited aerosol optical depths as high as 0.5 in the vicinity of the Maldives during the first half of March (Léon et al., 2001; Pelon et al., 2002). According to Ramanathan et al. (2001), emissions responsible of those high levels of pollution are mainly from anthropogenic origins (80%±10%).

2.2. Synoptic conditions during the first week of March 1999

Climatologically, there are two near-equatorial convergence zones in the Indian Ocean region: one in the northern hemisphere along 2°–5° N, which on average is less intense than the dominant convergence zone in the equatorial/southern Indian Ocean (Verver et al., 2001). During February, the northern convergence zone was more active, while in March the southern convergence zone became dominant, thereby favoring cross-equatorial flow and pollution transport from the northern hemisphere into the southern hemisphere.

In addition, the main features controlling the evolution of large scale circulation in the region of the INDOEX IFP domain (bounded by latitudinal limits between 30° N and 30° S, and longitudinally by 50° E and 100° E) during the first week of March were:

- the passage of tropical cyclone Davina, which formed on 2 March 1999 near 6° S, 100° E and moved southwestward, reaching Madagascar on 10 March 1999,
- the passage of two tropical depressions, one emerging west of northern Sumatra on 3 March, which deepened and moved westward and dissipated on 6 March 1999, the second developing southwest of Java on 5 March 1999 and following the track of Davina then on,
- the eastern shift of the subtropical high from central India to the Bay of Bengal

ACPD
5, 3269–3312, 2005

after 6 March 1999 as the Indian subcontinent began to heat up.

On 7 March 1999, northerly flow dominated over most of the Arabian Sea while offshore flow prevailed over coastal northeast India. The air parcels then curled anti cyclonically over the western Bay of Bengal around a weak high pressure. At 00:00 UTC, Davina was located 16° S, 75.5° E with the other tropical depression lying near 15° S, 93° E. Both the storms were southward of the southern hemisphere equatorial trough, which was reforming along 5°–7° S between 70°–95° E. The most intense convection was located near the tropical cyclone Davina and, as the northern hemisphere equatorial trough became active, over the equatorial Bay of Bengal with cloud clusters in the region along 0°–5° N and between 80°–100° E.

2.3. INDOEX-related operations on 7 March 1999

Besides the M-20, many other platforms specifically deployed in the framework of the INDOEX IFP operated on 7 March 1999. The Met Office C-130 Hercules aircraft flew to the west of the M-20 track, while the Indian Research Vessel Sagar Kanya (R/V SK) cruised along the western India coast line (see Fig. 1). In addition, a ground-based backscatter lidar was also operating at the site of Goa (Léon et al., 2002; Chazette, 2003).

Of interest to this study are the 12 dropsondes released by the Met Office C-130 and the 12 soundings on 7 March 1999. The position of the dropsondes and balloon releases are shown in Fig. 1. These shall be used to depict the thermodynamics of the monsoon layer over the Arabian Sea. Also shown in Fig. 1 are the locations of fifteen sounding stations of the dense Indian network, as data from the 00:00 and 12:00 UTC soundings shall be used (when available) for RAMS simulations validation purposes. Finally, airborne and ground-based backscatter lidar measurements made onboard the M-20 and at Goa, respectively, as well as ship-borne sun-photometer measurements made on the R/V SK shall be used to analyse the vertical structure and the diurnal evolution of the monsoon layer.

ACPD
5, 3269–3312, 2005

2.4. Airborne backscatter LIDAR measurements on 7 March 1999

The LIDAR observations of interest were acquired along one leg of the 7 March 1999 mission (the leg is referred to as FT1 in the following). FT1 was designed to be roughly oriented north-south. The position of this leg along which model fields have been extracted to compare with LIDAR measurements is shown in Fig. 1. LIDAR observations between 03:44 and 04:39 UTC (09:14–10:09 LT) are displayed in Fig. 2 in the form of the attenuated backscatter coefficient (ABC) (Pelon et al., 2002). The ABC, the product of the total (molecules and particles) backscatter coefficient of a given atmospheric layer and the two-way transmission between the aircraft and that layer, can be used to depict the horizontal and vertical structure of the aerosol plume over the Indian Ocean. The decrease in ABC near the surface, above of 8° N or in the presence of clouds at the top of the MABL, is related to lower two-way transmission values above these regions (i.e. aerosol or cloud scattering).

On this day, the vertical structure of the monsoon consisted of two layers: the MABL and the so-called land plume aloft. The cumulus clouds (characterized by ABC values larger than 5 km^{-1} sr^{-1}) were observed at the top of the MABL as well as embedded in the land plume. Such clouds may be considered as mixing elements between the MABL and the haze layer. These clouds eventually feed deeper clouds at the ITCZ (Manghnani et al., 2000). The depth of the MABL was relatively constant and varied between 400 and 500 m along the leg. On the other hand, the depth of the land plume exhibited larger fluctuations as a function of latitude. On 7 March, LIDAR observations of the haze plume above the MABL evidenced 3 regions (Fig. 2):

- a deep plume region: the land plume was observed to be deepest north of 8° N. The height of the top of the land plume was located at 2.7–3 km above mean sea level (m.s.l.). In this region, the height of the land plume top did vary by as much as 300 m,
- a shallow plume region: the land plume was observed to be most shallow south

ACPD
5, 3269–3312, 2005

of 7° N. The height of the land plume top varied between 1.4 and 1.8 km m.s.l.,

– a transition region: between 8° N and 7° N, the land plume top height decreased drastically with latitude from 3 km m.s.l. to 1.4 km m.s.l.

According to back trajectory analyses performed by Pelon et al. (2002), the air masses composing the elevated plume south of 7° N were coming from the Gulf of Bengal, whereas the air masses composing the deeper part of the plume (north of 8° N) were coming from the Indian sub-continent.

In Fig. 3a, we have plotted sequentially the potential temperature profiles obtained from the twelve dropsondes released between 05:19 and 07:34 UTC on 7 March 1999 (i.e. north of 8° N, in the region were the plume was observed to be the deepest). Except for the first one, profiles are being offet by +5 K with respect to the previous one. A marked potential temperature gradient is visible at an altitude varying between 2.9 and 3.3 km a.s.l. over the Arabian Sea (Fig. 3a), which corresponds to the depth of the aerosol plume observed by LIDAR. Backtrajectories computed using the NOAA HYSPLIT4 (National Oceanic and Atmospheric Administration Hybrid Single-Particle Lagrangian Integrated Trajectory) Model (Draxler and Hess, 1998) revealed that the air mass sampled with the dropsondes (below 4 km m.s.l.) was originating from Indian sub-continent. The temperature inversion was observed to be highest for the profile closest to the coast (i.e. Profile 5). Along the east-west oriented leg, there was evidence of subsidence as illustrated by the general trend of the elevated temperature inversion to lower and the associated potential temperature gradient to increase away from the coast. The depth of the MABL along the south-north oriented dropsonde leg (Profiles 1–5) was also found to be in good agreement with LIDAR observations. The MABL was deepest at the beginning of the east-west oriented leg (Profiles 6–8), its top reaching 1 km m.s.l. The MABL was observed to be well mixed on all profiles. The upper half of the elevated monsoon layer was also found to be well mixed, at least on the east-west oriented leg.

South of 6° N, the LIDAR-derived MABL and land plume height top were found in

agreement with the two temperature inversions evidenced in the 06:11 UTC sounding made in Kashidhoo, Maldives (Fig. 3b). The MABL was observed to be slightly deeper (700 m) than the one observed by LIDAR. This is believed to be caused by the influence of the land and related surface heating (recall that the sounding was made 3 h after the M20 overpass of Kashidhoo). Above the MABL, the lapse rate is about 5 K km^{-1} and the relative humidity decreases drastically from 90% to 20%. The base of the dry layer was observed at about 2 km m.s.l., an altitude where the lapse rate increased significantly. This is in fair agreement with the top of the pollution plume observed by LIDAR near 5° N.

3. Nested simulations using RAMS

RAMS version 4.3 (http://www.atmet.com) is a primitive equation prognostic, non-hydrostatic model developed for the simulation and forecasting of weather systems (Cotton et al., 2003). The cloud convection model included in RAMS model is the explicit scheme of Feingold et al. (1998). The model predicts soil temperature and moisture from the prognostic soil model which takes into account the vegetation cover and the type of soil (Walko et al., 2000). Many studies on regional pollution have used RAMS (e.g. Lyons et al., 1995; Millan et al., 1997; Edy and Cautenet, 1998; Cautenet et al., 1999; Audiffren et al., 2004; Taghavi et al., 2004).

Three simulations were performed: the one-grid simulation (run A), the two-grid reference simulation involves two nested domains (run B) while the sensitivity simulation (run C) has three nested domains. The location of the two or three nested grids is shown in Fig. 4. Information between the domains is exchanged two-ways using the scheme described in Clark et al. (1984) and Walko et al. (1995).

The largest domain, (grid 1) is bounded by meridians 58° E and 96° E, and by parallels 25° N and 8° S. This horizontal domain consists in 42×38 grid points, the mesh size being 100 km×100 km, and 35 sigma-z levels. The intermediate domain (hereafter referred to as grid 2) is centered on 77.5° E and 10° N. It is composed of 152×152 points

ACPD
5, 3269–3312, 2005

with a horizontal mesh size of 20 km×20 km. The smallest domain (grid 3) has a horizontal resolution of 5 km×5 km and it is centered in 76° E and 8.5° N. The time steps are 30, 6 and 1.5 s for grid 1, grid 2 and grid 3, respectively. The choice of the vertical resolution has been a critical point of the simulation. Indeed, preliminary simulations have shown that the vertical resolution should be high enough to correctly capture the dynamical processes ongoing along the western coastline due to the presence of orography. Hence, we have chosen 35 vertical levels for the grid 1 and 62 levels for grids 2 and 3 between the ground and 22 km m.s.l. Vertical levels are designed in (σ, p) coordinates. With such configuration we have 39 levels below 4000 m m.s.l. for grid 2 and 3, with a resolution on the order of 300 m at 4000 m m.s.l.

The grid 1 simulation was driven by ECMWF (European center for Medium-Range Weather Forecasts) re-analyses (available every 6 h). The simulation begins at 00:00 UTC on 26 February and ends at 12:00 UTC on 9 March 1999.

The 1-km resolution soil vegetation model (important to capture the breeze circulations over land) from USGS (United States Geophysical Survey) is used to described land use in the simulation. In the model, the topography is obtained by interpolating the available 1-km resolution database to the mesh size of the nested domains. The sea surface temperature used in the model is based upon monthly climatologically data at 1°×1° resolution available from the ATMET database.

For this study, it is crucial that the dynamics in the simulation be as realistic as possible in order for the model to reproduce the monsoon haze plume. The horizontal wind fields (wind barbs) simulated on the intermediate domain (grid 2) at 00:00 and 12:00 UTC on 7 March and at two levels (850 hPa and 500 hPa) are shown in Fig. 5. Also shown are the wind barbs extracted at these levels from the upper air soundings of the Indian network (see Fig. 1 for locations) when available. It can be seen that the agreement between the wind fields from RAMS simulations at 00:00 and 12:00 UTC are in very good agreement with the observations at 500 hPa (Fig. 5a, b). The agreement is also good at the 850 hPa (Fig. 5c, d), except maybe in some locations along the western coast where the influence of the Ghats may generate local circulation that

cannot necessarily be reproduced with the simulation. Nevertheless, the worse agreement is found over central India, in a region located near the center of the continental anticyclone where winds are generally weak (e.g. in Aurangabad at 00:00 UTC or Nagpur at 12:00 UTC). The general agreement between observations and simulations in terms of dynamics was found to be good throughout the period of the simulation (not shown). This is crucial since the structure of tracer plume observed on 7 March 1999 is conditioned by the history of the airmasses for as long as 7 to 10 days.

4. Tracer simulations

To analyse the 3-D structure of the Indo-Asian haze plume over the Arabian Sea, north of the Maldives, passive tracer sources, corresponding to 4 important emission areas, have been introduced. They have been selected based on the back-trajectory analyses performed by Pelon et al. (2002) for the 7 March 1999 case. The 4 emission regions are centered on Calcutta (88.45° E; 22.65° N), Bombay (72.85° E; 19.11° N), Hyderabad (78.46° E; 17.45° N), and Madras (80.18° E; 13° N), respectively (see Fig. 4) and are hereafter referenced as R1, R2, R3, R4. Emission rates are prescribed to be steady with time and to be consistent with the EDGAR database: emission rates in R1 and R2 are prescribed to be the same, whereas emission rates in R3 and R4 are prescribed to be 75% of those in R1 and R2. In the following, tracer concentrations are expressed in arbitrary unit (a.u.). The objective is to assess whether the structure of the haze plume observed by LIDAR to the north and to the west of the Maldives Islands on 7 March 1999 can be reconstructed based on tracer simulations from the above mentioned sources.

4.1. Origin of pollutants composing the haze plume sampled by LIDAR

Based on LIDAR observations on 7 March 1999, we have selected 2 altitude levels to look at the circulation patterns and the transport of aerosols from the continental

sources: 100 m m.s.l. (in the MABL) and 2 km m.s.l. (at this level, haze was observed in both the shallow and deep plume region).

Figure 6 shows the horizontal distribution of tracer concentration (at 03:00 UTC) associated with individual plumes emitted from R1, R2, R3, R4 after 9 days of simulation, at 100 m m.s.l., on grid 2 of the reference numerical experiment (run B) with superimposed horizontal wind vectors. The northern convergence zone is clearly seen along 0–5° N between 65° E and 90° E, associated with the strong northeasterly and northerly outflows over the Arabian Sea and Gulf of Bengal, respectively. Tracers are simulated to be transported to the southwest of the Indian sub-continent as far as 2000 km from their emission sources after 9 days. The plume of pollutants can be visualized as the region where the tracer concentrations are larger than 5 arbitrary unit (a.u., set arbitrarily). The plumes from Calcutta and Bombay were simulated to travel over the ocean for the most part (Gulf of Bengal and Arabian Sea, respectively) (Fig. 6a and b) whereas plumes from Madras and Hyderabad (Fig. 6c and d) were simulated to travel over the Indian sub-continent prior to being advected over the Arabian Sea. It is worth noting that, even though most of the plume from Calcutta traveled over the Gulf of Bengal, the northern portion of it (i.e., the portion arriving over the M-20 track) had traveled partly over the continent. As discussed later, the vertical distribution of tracer concentration in the plumes originating from Madras and Hyderabad (and to a lesser extent the northern portion of the Calcutta plume) were impacted by the diurnal cycle of convection over land. At this height, it appears from the simulations that the aerosols sampled by LIDAR along FT1 in the MABL were associated with the plume from Madras and Calcutta.

Figure 7 shows the horizontal distribution of tracer concentration (at 03:00 UTC) associated with individual plumes emitted from R1, R2, R3, R4, after 9 days of simulation, at 2000 m m.s.l. Here also the northern convergence zone is clearly seen along 0–5° N between 65° E and 77.5° E over the Arabian Sea. The subtropical high is seen over northeastern Indian, while another anticyclonic feature is seen offshore from the Indian west coast over the Arabian Sea (the same features are also simulated

at 3500 m m.s.l., not shown). An interesting feature of the simulation at this height is the presence of a region of "accumulation" of tracers from all sources (but mostly from Calcutta) between 5° N and 5° S. This is due to the lack of adequate in-cloud wash-out process of passive tracers in the model. The consequence is that these tracers are ventilated from MABL by deep convection in the northern convergence zone where they should be scavenged. In Fig. 8a, we display the liquid water mixing ratio simulated by the model on 7 March 1999 at 03:00 UTC. The patterns of enhanced precipitation, associated with deep convection (marking the position of northern convergence zone in the simulation), is well correlated with the patterns of tracers south of 5° N. This is further confirmed by the NOAA 15 infrared image over the Indian Ocean at 03:09 UTC on 7 March 1999 (Fig. 8b) which shows the presence of elevated clouds approximately where the convergence zone occurs in the simulated wind field (Fig. 7). The high concentrations of tracers simulated along the Indian western coastline in Fig. 7c and d are connected to the explosive combination of breeze and orographic lifting (cf. Sect. 2.2). As discussed later on the basis of the simulations, this effect is maximum at 12:00 UTC on the continent. Simulations emphasize that tracers from Calcutta, Madras and Hyderabad are re-circulated in the sea breeze cell of the west coast as shown in Fig. 7a, c and d. At this height also, it appears from the simulations that the aerosols sampled by LIDAR along FT1 above the MABL were mainly associated with plumes from Madras and Hyderabad, and to a lesser extend with the plume from Calcutta.

4.2. Vertical structure of the simulated plume

The vertical distribution of tracer concentration (a proxy of the structure of the plume) along the M-20 flight track (FT1) obtained from the 2-grid reference simulation (run B) on grid 2 is shown in Fig. 9a. This tracer concentration field is obtained by summing the individual tracer fields from all 4 emission sources. In order to ensure meaningful comparison of the tracer concentration cross-section with the LIDAR-derived ABC cross-section, one must be aware that careful analysis of the relative humidity (*RH*) field is essential (Fig. 9b). For hydrophilic aerosols (such as MABL aerosols), it is gen-

erally considered that above *RH* values of 75%, aerosol size swells by absorption of water vapor which leads to a drastic modification of the aerosol optical properties. For such aerosols, LIDAR ABC is generally observed to increase with *RH* for a well-mixed concentration profile. For hydrophobic aerosols (such as the pollution aerosols transported from the Indian sub-continent; Cantrell et al., 2000, 2001; Chazette, 2003), *RH* has little impact on the aerosol scattering properties. Hence maximum values in the LIDAR ABC field can be interpreted as maximum values in aerosol concentration (which is not a sound hypothesis in the MABL).

In the simulation, the MABL is identified as the layer characterized by high *RH* (90% or more) and large tracer concentration (the highest tracer concentrations are found in the MABL). The depth of the MABL decreases with increasing latitude, from 1500 m to the south to 600 m to the north (Fig. 9b). Aloft, in the haze plume, the *RH* is less than 40% around 2 km m.s.l. In the southern part of the transect (FT1), *RH* increases near the top of the plume where higher clouds are simulated. This is in good agreement with the *RH* measurements made over Male with the M-20 which showed that *RH* varied between 60 and 80% near the surface, reaching values of 95% or more at the MABL top. Aircraft measurements in the plume aloft revealed that *RH* was on the order of 40%, except near the top of this layer where *RH* increased sharply to 80%, as generally observed in winter monsoon flows (Mohanty et al., 2000; Manghnani et al., 2000).

In the following, we define the altitude of the top of the plume as the altitude of iso-contour 5 a.u. (this allowed for the most realistic simulation-derived plume structure when compared to airborne LIDAR measurements). North of 6° N, the general structure of the plume is reasonably simulated, even though the altitude of the top of the plume is approximately 400 m too low for the northern part of the transect (where the observed plume is thicker). Furthermore, the maximum of LIDAR-derived ABC (related to a maximum of aerosol concentration and/or *RH*) observed between 8° N and 9° N around 2.25 km m.s.l. is not simulated. This could be due to the coarse representation (i.e. a mesh size of 20 km) of the coastal dynamics resulting in a weaker vertical development of the CBL as discussed in the next section. However, the top of the land plume defined

by the *RH* increase (40% to 80%) is consistent with LIDAR observations. As *RH* has a non negligible effect on LIDAR ABC, one has to be careful when comparing simulation-derived tracer fields with LIDAR-derived ABC fields.

South of 6° N, the tracer plume is deeper than observed by LIDAR. However, the interpretation of the concentrations simulated in the southern part of transect is difficult. As shown in Fig. 7, the southern part of FT1 is embedded in the northern convergence zone. Hence, in the simulation, strong convective towers transport the tracers in altitude. Because there are no scavenging processes for tracers in the model, they accumulate in this region. The consequence is an overestimation of tracer concentration and vertical flux. The presence of the northern convergence zone in this region also explains the deeper MABL and the poor agreement between the observed structure and the simulated one. LIDAR observations (Fig. 2) do not suggest the presence of the northern convergence zone as far north as 5–6° N. Hence it is not believed that in this region the comparison of simulated and observed ABC will be in agreement.

4.3. Tracer plume diurnal evolution and propagation over the ocean

During the daytime, the combination of sea breeze circulation and orographic lifting induced by the presence of the Western Ghats (a mountain ridge of moderate height running along the western coast of India) has a profound influence on the structure of the land plume (Mohanty et al., 2000; Roswintiarti et al., 2001; Léon et al., 2001; Ethé et al., 2002). Krishnamurti et al. (1998) have suggested that the depth of the elevated pollution plume transported over the ocean was controlled by the diurnal variability of the Continent Boundary Layer (CBL) and the height of the trade wind inversion layer. This was confirmed by LIDAR measurements made in Goa during the IFP (Chazette, 2003) which evidenced the diurnal cycle of the AOD and extinction coefficient profiles. Along the Indian west coast, the altitude of the top of the pollution plume varied between 3 and 4 km m.s.l., the deeper plume depths being observed at 12:00 UTC (Chazette, 2003). Continental aerosols are generally observed to be mixed on the vertical throughout the depth of this land plume (Léon et al., 2001; Raman et al., 2002).

ACPD
5, 3269–3312, 2005

Temperature profiles obtained from synoptic balloon sounding in Goa during the period running from 6 to 9 March 1999 show the presence of an elevated temperature inversion at this level, fluctuating between 3 and 4 km m.s.l. (not shown). This is also seen on dropsonde measurements performed west of the continent by the Met Office C-130 (Fig. 3a). A maximum height of the inversion is observed on profile 5, which is the closest to the shoreline (see Fig. 2). Other profiles show a lower inversion altitude which can be attributed to large scale subsidence. During the night, such explosive combination of breeze and orographic lifting is generally not observed so that the CBL is much shallower.

During the period from 12:00 UTC on 5 March to 12:00 UTC on 9 March 1999, the impact of coastal dynamics on the aerosol plume spatio-temporal structure is well marked. This is illustrated in Fig. 10 where we show a vertical cross-section of the tracer concentration (u.a.) at 10° N latitude and between 73° E and 78.5° E obtained with the 2-grid reference simulation (run B) every 6 h from 00:00 UTC on 6 March 1999 to 18:00 UTC on 7 March 1999. A 24 h periodic cycle takes place of which main phases can be describe as: (i) strong vertical development of the aerosol plume over the continent with a maximum between 12:00 and 15:00 UTC; (ii) horizontal advection of the land plume over the ocean by the winter monsoon flow (15:00–00:00 UTC) and (iii) subsidence of the plume over the ocean (00:00–12:00 UTC).

Unfortunately, very little observations were available during INDOEX to verify the validity of this proposed scheme over the Arabian Sea. Even though, the influence of this diurnal variability on the optical properties of the continental plume has been highlighted on Meteosat images in the form of a frontal discontinuities in the brightness surface temperature fields oriented parallel to and propagating away from the coastline (Désalmand et al., 2003), little relevant information on the vertical structure of the pollution plume and its evolution over the sea was available. A three day sun-photometer AOD sequence acquired from the R/V SK close to the west Indian coast (see Fig. 1) proved to be more reliable for observing of the diurnal cycle of the optical properties of the pollution plume (the R/V SK was cruising slowly along the coast). We also have

used the LIDAR measurements made in Goa (Chazette, 2003) for validation purpose in the coastal region of India.

For comparison with available LIDAR and sun-photometer datasets, we display the temporal variations of simulated concentrations at 2000 m m.s.l. (upper part of the plume) at four locations (P1 through P4) along a transect approximately perpendicular to the west Indian coast and roughly parallel to the mean wind direction at 2000 m m.s.l. (see Fig. 11) for this period. The four locations are equidistant.

The tracer concentration at 2000 m m.s.l. at the coastal site (P1, 76.5° E/10° N) exhibits a well established diurnal cycle with maximum values at about 12:00–15:00 UTC and minimum values at 06:00 UTC, consistent with the first two phases described above (Fig. 12). Furthermore, maxima (minima) of LIDAR-derived aerosol extinction coefficient observed at this height in Goa occur at the same time as in the simulation, i.e. around 12:00 (06:00) UTC (Fig. 13). For a given day, the concentration build-up phase (06:00–15:00 UTC) is always shorter than the concentration decay phase (15:00–06:00 UTC). This is also in remarkable agreement with the extinction coefficient at 2000 m m.s.l. (Fig. 13) for a period running from 1 to 8 March 1999. The extinction coefficient is observed to increase more rapidely than it decreases in the course of the diurnal cycle. Hence, the diurnal evolution of the observed extinction coefficient and the simulated tracer concentration are strikingly similar. Recall that the pollution aerosols produced by India were shown to be hydrophobic, and hence both quantities can be compared directly. In Fig. 12, it is also worth noting the increase in concentration in P1 from 6 to 8 March, on the order of 20%. This is not caused by enhanced emissions over the continent as in the simulation the emissions are constant. This significant increase is also not believed to be due to accumulation (caused by the lack of dry deposition in the simulation), as dry deposition at this level (2000 m m.s.l., above the MABL) is likely to be insignificant. Furthermore the strength of the flow at this level (10 m s^{-1} or more) is likely to act against accumulation, leading to rapid dispersion of the pollutants. Rather, we propose the following explanation. A fraction of the tracers that are transported over ocean in altitude by the monsoon flow when the land breeze

is well established undergo subsidence over the ocean and/or are mixed in the MABL via the entrainment process. The next day when the land breeze establishes again, the tracers that have been entrained in the MABL are advected in the landward (southwesterly) branch of breeze circulation and mix, in the region of the Western Ghats, with the freshly produced tracers advected northeasterly from the continent. This hypothesis is "apparently" not corroborated by the LIDAR measurements in Goa, Fig. 13 showing that the maximum of extinction coefficient remained almost unchanged between 1 and 8 March. Léon et al. (2001) evidenced that the maximum of aerosol extinction coefficient in the monsoon layer observed in Goa was the result of accumulation of pollution aerosols transported from remote sources. This cannot be accounted for in our fairly idealized tracer simulation. In the absence of emission sources over the continent, our results are strongly influenced by the local pollution sources (such as Madras). Considering that our tracer simulation results are only representative of local dispersion/build-up processes, it can be argued that these processes only account for a small fraction of the aerosol load otherwise observed in Goa. In this context, results from the idealized tracer simuation are not necessarily incompatible with the fact that the maximum of extinction coefficient remained almost unchanged between 1 and 8 March. Rather we have identified a plausible re-circulation mechanism likely to be important at the local scale along the western Indian coastline, but which contribution to the total aerosol load may be small, and hence difficult to isolate from observations only.

For the first cycle (6–7 March), the tracer concentration at the P2 (74.3° E/9.3° N) and P3 (72.7° E/8.6° N) exhibits the same diurnal cycle as P1, with a shift of 6 h and 12 h, respectively. Interestingly, over the ocean, the tracer concentration evolution is reminiscent of a propagating front. The propagation speed between P1 and P3 is relatively constant and on the order of 13 m s^{-1}, consistent with the propagation speed of cloud bands traveling westward over the Arabian Sea ahead of the Indian pollution plume assessed using Meteosat-5 imagery (Désalmand et al., 2003). In P4 (69.9° E/7.6° N), a slight increase in tracer concentration is seen at 0600 UTC on 7

March, that is not necessarily associated with the propagating tracer plume. During the second cycle (7–8 March), the tracer concentration in P1, P2 and P3 exhibits the same general trend than during the first cycle, the propagation speed of the tracer plume also being on the order of 13 m s^{-1} between P1 and P3. During the third cycle (8–9 March), resembles that of the two others, except that the signature of the arrival of the tracer plume in P3 is weak during that cycle. During the period under scrutiny, there is also a significant correlation between what is simulated in P4 and in the other locations, suggesting long range transport of tracers in the simulation.

In Fig. 14, we show the AOD derived from a photometer installed on the R/V SK for a period ranging from 5 to 8 March 1999, close to the coastline (see Fig. 1). During this period, the R/V SK equivalent distance to the coast is comprised between P2 and P3. The strong AOD diurnal cycle is evident, suggesting large diurnal fluctuations of the aerosol content in the monsoon layer over the Arabian Sea, in agreement with tracer concentration variations in P2 and P3.

4.4. Sensitivity experiment

To investigate the impact of grid resolution on the vertical structure of the simulated plume, we compare vertical winds and the structure of the tracer plume on a transect running along latitude 10 °N on the Indian sub-continent, between 73° E and 79° E, resulting: (i) from run A on grid 1 (referred to as S1, Fig. 15a and b), (ii) from run B on grid 2 (referred to as S2, Fig. 15c and d), and (iii) from run C on grid 2 (referred to as S3, Fig. 15e and f). The simulation results shown in Fig. 15 are obtained for the sum of the 4 emission sources and correspond to 6 March 1999 at 12:00 UTC where the vertical development of continental plume is maximum.

It is obvious that the explosive combination of sea breeze and orographic lifting over Indian west coast is more efficient for S3 than for S1. This is likely related to the fact that over land, vertical motion resulting from the combination of sea breeze and orographic lifting is enhanced in S3 due to higher resolution, less smooth dynamics and orography, and more realistic wind fields. Indeed, where vertical velocities never exceed values

of 5 cm s^{-1} in S1 (characteristic of GCM resolutions; Fig. 15a), they can reach values of 15 cm s^{-1} in S2 (configuration used in Sects. 4.1 and 4.2; Fig. 15b) and values of 30 cm s^{-1} in S3 along the western ridges of the Ghats. As a consequence, tracers are injected higher in the troposphere over the Western Ghats, the top of the tracer plume reaching 3.5 km m.s.l. (Fig. 15f). Over the ocean, the depth of the plume decreases (slightly) with increasing resolution.

In Fig. 16, we show the vertical distribution of tracer concentration along FT1 obtained from the high resolution simulation in grid 3 (run C) on 7 March 1999 at 03:00 UTC. The tracer concentration field in Fig. 16 is obtained by summing the individual tracer fields from all 4 emission sources. Comparing to the distribution from S2 (Fig. 9a) and to the observation (Fig. 2), the structure of the plume is globally better retrieved at the exception of the southern part, due to the presence of the northern convergence zone in the simulation as discussed earlier. On the other hand, the tracer concentration maximum simulated at 2000 m m.s.l. between 8° N and 9° N and the associated minimum below is reminiscent of the LIDAR ABC structure observed in this region. It is the consequence of the better representation of coastal dynamics.

5. Summary and conclusion

Three-dimensional nested tracer simulations of a pollution plume transported from the Indian sub-continent over the Indian Ocean in the framework of INDOEX between 5 and 9 March 1999 were performed with RAMS. These simulations provide insight into the transport patterns of the pollutants as well as investigate the dynamical mechanisms controlling the vertical structure of the plume and its evolution in the vicinity of the Maldives Islands. Airborne and ground-based LIDAR observations of the structure of the haze plume made on 7 March 1999 were used to assess the quality of the simulations as well as the impact of grid resolution on the vertical structure of the simulated plume. Twelve dropsondes released by the Met Office C-130, ground-based backscatter LIDAR measurements made at Goa, respectively, as well as ship-borne

sun-photometer measurements made on the R/V SK were also used in this study.

The focus of this paper is to validate the high resolution simulations of 3-D structure of the plume obtained with the RAMS over the Indian Ocean in the vicinity of the Maldives Islands using LIDAR measurements. At this point we have only considered passive tracers as a proxy for anthropogenic aerosols. We also have not considered the whole Indian sub-continent as a source region, but we rather have selected 4 cities (Bombay, Madras, Hyderabad and Calcutta) as the major emission sources. This exercise is nearly impossible to do basing on realistic emissions of "real aerosols" because sources are numerous and aerosols cannot be tagged to their sources. Our objective is to determine the origin of the aerosol composing the plume observed by LIDAR on 7 March 1999 (Pelon et al., 2002) and to assess whether the transport patterns leading to the simulated vertical structure of the plume are consistent with observations.

The main results can be summarized as follow:

- Downwind to the Western Ghats, over the Arabian Sea, a strong two-layered structure composed by the MABL and the land plume aloft observed by LIDAR measurements was realistically simulated with RAMS. According to tracer simulations, the aerosols observed in the land plume came from the southern Indian sub-continent. Within the MABL, pollutants come mainly from the southern Indian continent and Calcutta (below 6° N), and to a lesser extent from Bombay and the northern Indian sub-continent (above 10° N),

- As far as 600 km from Indian coast, the vertical structure of the plume exhibits a sharp diurnal cycle, as shown with the tracer simulations. Closer to the coastline, ground-based LIDAR (aerosol extinction coefficient) and ship-borne sun-photometer AOD measurements also evidenced a well marked diurnal cycle of aerosol optical properties. The observed and simulated diurnal cycles are in excellent agreement,

- Local scale dynamical processes near the coast, as well as entrainment at the top of the marine atmospheric boundary layer, also play a crucial role in re-circulating

a fraction of the tracers transported over ocean by the winter monsoon flow above the marine atmospheric boundary layer in the landward (southwesterly) branch of breeze circulation during the following day, which, in turn, leads to pollutant accumulation in the vicinity of the Indian coastline. Nevertheless, this contribution to the total aerosol load observed during the INDOEX IFP may be small compared to that related to massive advection of aerosol from the continent (which is not accounted for here),

– The nesting of a high horizontal resolution domain (5 km, with 39 vertical levels below 4000 m m.s.l.) allows a better representation of local dynamics, sea breeze circulation, and therefore a noticeable improvement in the representation of the pollutants plume.

Based on the encouraging preliminary simulation results obtained in this paper, the next step (the focus of a companion paper) will be to proceed with the realistic simulation of the haze plume and (i) to validate the 3-D structure of the plume using LIDAR observations and (ii) to compute (using Mie theory) the extinction and backscatter coefficient profiles based on simulated aerosol concentrations and distributions and finally, to compare them with their LIDAR-derived counterparts. This shall be done on the high horizontal resolution domain (5-km) rather than the 20-km resolution domain. We believe that only a comparison of synthetic ABC fields (resulting from realistic aerosol simulation as aimed at in a companion paper) with LIDAR-derived ABC fields would be considered satisfying and meaningful.

Acknowledgements. This work was supported by funding of the Centre National de la Recherche Scientifique through the Programme National de Chimie Atmosphérique (PNCA) and the Programme Atmosphère et Océan à Moyenne Echelle (PATOM). Mystere 20 operations were supported by the European Space Agency (ESA). This work makes a large use of the RAMS model, which was developed under the support of the National Science Foundation (NSF) and the Army Research Office (ARO). Computer ressources were provided by CINES (Centre Informatique National de l'Enseignement Supérieur) project amp2107. The authors also wish to thank the computer team of the Laboratoire de Météorologie Physique

de l'Université Blaise Pascal (France): A. M. Lanquette, P. Cacault and F. Besserve. Finally, A. Jayaraman is acknowledged for permission to use the ship-borne sun-photometer data.

References

Audiffren, N., Buisson, E., Cautenet, S., and Chaumerliac, N.: Photolytic impact of a stratocumulus cloud layer upon the chemistry of an offshore advected plume of pollutants during the NARE 1993 intensive experiment: a numerical study, Atmos. Res., 70, 89–108, 2004.

Cantrell, W., Shaw, G., Cass, G., Chowdhury, Z., Hughes, L., Prather, K., Guazzotti, S., and Coffee, K.: Closure between aerosol particles and cloud condensation nuclei at Kaashidhoo Climate Observatory, J. Geophys. Res., 106, 28 711–28 718, 2001.

Cantrell, W., Shaw, G., Leck, C., Granat, L., and Cachier, H.: Relationships between cloud condensation nuclei spectra and aerosol particles on a south-north transect of the Indian Ocean, J. Geophys. Res., 105, 15 313–15 320, 2000.

Cautenet, S., Poulet, D., Delon, C., Delmas, R., Grégoire, J. M., Pereira, J. M., Cherchali, S., Amram, O., and Flouzat, G.: Simulation of carbon monooxide redistribution over Central Africa during biomass burning (Experiment for Regional Sources and Sinks of Oxidants (EXPRESSO)), J. Geophys. Res., 104, 30 641–30 657, 1999.

Chazette, P.: The monsoon aerosols extinction properties at Goa during INDOEX as measured with lidar, J. Geophys. Res., 108, doi:10.1029/2002JD002074, 2003.

Clark, T. L. and Farley, R. D.: Severe downslope windstorm calculations in two and three spatial dimensions using anelastic interactive grid nesting: A possible mechanism for gustiness, J. Atmos. Sci., 41, 329–350, 1984.

Cotton, W. A., Pielke, R. A., Walko, R. L., Liston, G. E., Tremback, C. J., Jiang, H., McAnelly, R. L., Harrington, J. Y., Nicholls, M. E., Carrio, G. G., and McFadden, J. P.: RAMS 2001: Current status and future directions, Meteorol. Atmos. Phys., 82, 5–29, 2003.

Désalmand, F., Szantai, A., Picon, L., and Desbois, M.: Systematic observation of westward propagating cloud bands over the Arabian Sea during Indian Ocean Experiment (INDOEX) from Meteosat-5 data, J. Geophys. Res., 108, doi:10.1029/2002JD002934, 2003.

Draxler, R. R. and Hess, G. D.: An overview of the Hysplit_4 modeling system for trajectories, dispersion, and deposition, Aust. Met. Mag., 47, 295–308, 1998.

Edy, J. and Cautenet, S.: Biomass burning : local and regional redistributions, Air Pollution Modeling and its application, Plenum Press, New-York, 63–69, 1998.
Ethé, C., Basdevant, C., Sadourny, R., Appu, K. S., Harenduprakash, L., Sarode, P. R., and Viswanathan, G.: Air mass motion, temperature, and humidity over the Arabian Sea and western Indian Ocean during the INDOEX intensive phase, as obtained from a set of super-pressure drifting balloons, J. Geophys. Res., 107, doi:10.1029/2001JD001120, 2002.
Feingold, G., Walko, R. L., Stevens, B., and Cotton, W. R.: Simulation of marine stratocumulus using a new microphysical parameterization scheme, Atmos. Res., 47–48, 505–528, 1998.
Franke, K., Ansmann, A., Müller, D., Althausen, D., Venkataraman, C., Reddy, M. S., Wagner, F., and Scheele, R.: Optical properties of the Indo-Asian haze layer over the tropical Indian Ocean, J. Geophys. Res., 108, doi:10.1029/2002JD002473, 2003.
Huebert, B. J., Bates, T., Russell, P. B., Shi, G., Kim, Y. J., Kawamura, K., Carmichael, G., and Nakajima, T.: An overview of ACE-Asia: Strategies for quantifying the relationships between Asian aerosols and their climatic impacts, J. Geophys. Res., 108, doi:10.1029/2003JD003550, 2003.
Krishnamurti, T. N., Jha, B., Prospero, J., Jayaraman, A., and Ramanathan, V.: Aerosol and pollutant transport and their impact on radiative forcing over the tropical Indian Ocean during the January-February 1996 pre-INDOEX cruise, Tellus B, 50, 521–542, 1998.
Lelieveld, J., Crutzen, P. J., Ramanathan, V., Andreae, M. O., Brennikmeijer, C. A. M., Campos, T., Cass, G. R., Dickerson, R., Fischer, H., De Gouw, J. A., Hansel, A., Jefferson, A., Kley, D., De Laat, A. T. J., Lal, S., Lawrence, M. G., Lobert, J. M., Mayol-Bracero, O. L., Mitra, A. P., Novakov, T., Oltmans, S. J., Prather, K. A., Rodhe, H., Scheeren, H. A., Sikka, D., and Williams, J.: The Indian Ocean Experiment : Widespread air pollution from South and South East Asia, Science, 292, 1031–1036, 2001.
Léon, J.-F., Chazette, P., Dulac, F., Pelon, J., Flamant, C., Bonazzola, M., Foret, G., Alfaro, S., Cachier, H., Cautenet, S., Hamonou, E., Gaudichet, A., Gomes, L., Rajot, J.-L., Lavenu, F., Inamdar, S. R., Sarode, P. R., and Kadadevarmath, J. S.: Large-scale advection of continental aerosols during INDOEX, J. Geophys. Res., 106, 28 427–28 439, 2001.
Lohmann, U. and Feichter, J.: Can the direct and semi-direct aerosol effect compete with the indirect effect on a global scale?, Geophys. Res. Lett., 28, 159–161, 2001.
Lyons, A. W., Tremback, C. J., and Pielke, R. A.: Applications of the regional atmospheric systems (RAMS) to provide input to photochemical grid models for the lake Michigan ozone study (LMOS), J. Appl. Meteor., 34, 1762–1785, 1995.

Mahapatra, A. S. and Michel, C. P.: Biofuel consumption, deforestation, and farm level tree growing in rural India, Biomass bioenergy, 17, 291–303, 1999.

Manghnani, V., Raman, S., Nyogi, D., Parameswara, V., Morrison, J., Ramana, S. V., and Raju, J.: Marine boundary-layer variability over the Indian Ocean during INDOEX (1998), Boundary Layer Meteorol., 97, 411–430, 2000.

Millan, M. M., Salvador, R., Mantilla, E., and Kallos, G.: Photooxidant dynamics in the smtag307 Mediterranean basin in summer: Results from European research projects, J. Geophys. Res., 102, 8811–8823, 1997.

Mohanty, U., Niyogi, D., Raman, S., and Sarkar, A.: Numerical simulation of land-air-sea interactions over the Indian ocean during the northeasterly Monsoon during INDOEX, Curr. Sci., 80, 60–68, 2001.

Pelon, J., Flamant, C., Chazette, P., Léon, J.-F., Tanre, D., Sicard, M., and Satheesh, S. K.: Characterization of aerosol spatial distribution and optical properties over the Indian Ocean from airborne LIDAR and radiometry during INDOEX'99, J. Geophys. Res., 107, doi:10.1029/2001JD000402, 2002.

Raes, F., Bates, T., McGovern, F. M., and Van Liederkerte, M.: The second Aerosol Characterization Experiment (ACE-2): general overview and main results, Tellus, 52B, 111–126, 2000.

Raman, S., Devdutta, D., Niyogi, S., Simpson, M., and Pelon, J.: Dynamic of the elevated land plume over the Arabian Sea and the Northern Indian Ocean during northeasterly monsoons and during the Indian Ocean Experiment (INDOEX), Geophys. Res. Lett., 29, doi:10.1029/2001GL014193, 2002.

Ramanathan, V., Chung, C., Clarke, A., Coakley, J., Collins, W., Conant, W., Dulac, F., Heintzenberg, J., Heymsfield, A., Holben, B., Howell, S., Crutzen, P., Hudson, J., Jayaraman, A., Kiehl, J., Krishnamurti, T., Lubin, D., McFarquhar, G., Novakov, T., Ogren, J., Podgorny, I., Prather, K., Lelieveld, J., Priestley, K., Prospero, J., Quinn, P., Rajeev, K., Rasch, P., Rupert, S., Sadourny, R., Satheesh, S., Shaw, G., Sheridan, P., Mitra, A., Valero, F., Althausen, D., Anderson, J., Andreae, M., Cantrell, W., and Cass, G.: Indian Ocean Experiment: An integrated analysis of the climate forcing and effects of the great Indo-Asian haze, J. Geophys. Res., 106, 28 371–28 398, 2001.

Rasch, P. J., Collins, W. D., and Eaton, B.: Understanding the Indian Ocean Experiment (INDOEX) aerosol distributions with an aerosol assimilation, J. Geophys. Res., 106, 7337–7355, 2001.

Reiner, T., Sprung, D., Jost, C., Gabriel, R., Mayol-Bracero, O. L., Andreae, M. O., Campos, T. L., and Shetter, R. E.: Chemical characterization of pollution layers over the tropical Indian Ocean: Signatures of emissions from biomass and fossil fuel burning, J. Geophys. Res., 106, 28 497–28 510, 2001.

Roswintiarti, O., Raman, S., Mohanty, U. C., and Niyogi, D.: Application of three-dimensional triple nested mesoscale model for assessing the transport and boundary layer variability over the Indian Ocean during INDOEX, Curr. Sci., 80, 69–76, 2001.

Russell, P. B., Hobbs, P. V., and Stowe, L. L.: Aerosol and radiative effects in the United States east coast haze plume : An overview of the tropospheric Aerosol radiative Forcing Observational experiment (TARFOX), J. Geophys. Res., 104, 2213–2222, 1999.

Sinha, C. S., Sinha, S., and Josh, V.: Energy use in the rural areas of India: setting up a rural energy database, Biomass bioenergy, 14, 489–503, 1998.

Streets, D. G. and Waldhoff, S. T.: Greenhouse-gas emission from biofuel combustion in Asia, Energy, 24, 841–855, 1999.

Taghavi, M., Cautenet, S., and Foret, G.: Simulation of ozone production in a complex circulation region using nested grids, Atmos. Chem. Phys., 4, 825–838, 2004, SRef-ID: 1680-7324/acp/2004-4-825.

Verver, G. H. L., Sikka, D. R., Lobert, J. M., Stossmeister, G., and Zachariasse, M.: Overview of the meteorological conditions and atmospheric transport processes during INDOEX 1999, J. Geophys. Res., 106, 28 399–28 413, 2001.

Walko, R. L., Tremback, C. J., Pielke, R. A., and Cotton, W. R.: An interactive nesting algorithm for stretched grids and variable nesting ratios, J. Apl. Meteor., 34, 994–999, 1995.

Walko, R. L., Band, L. E., Baron, J., Kittel, T. G., Lammers, R., Lee, T. J., Ojima, D., Pielke Sr., R. A., Taylor, C., Tague, C., Tremback, C. J., and Vidale, P. L.: Coupled atmosphere-biophysics-hydrology models for environmental modelling, J. Appl. Meteor., 39, 931–944, 2000.

Welton, E. J., Voss, K. J., Quinn, P. K., Flatau, P. J., Markowicz, K., Campbell, J. R., Spinhirne, J. D., and Gordon, H. R.: Measurements of aerosol vertical profiles and optical properties during INDOEX 1999 using micropulse lidars, J. Geophys. Res., 107, doi:10.1029/2000JD000038, 2002.

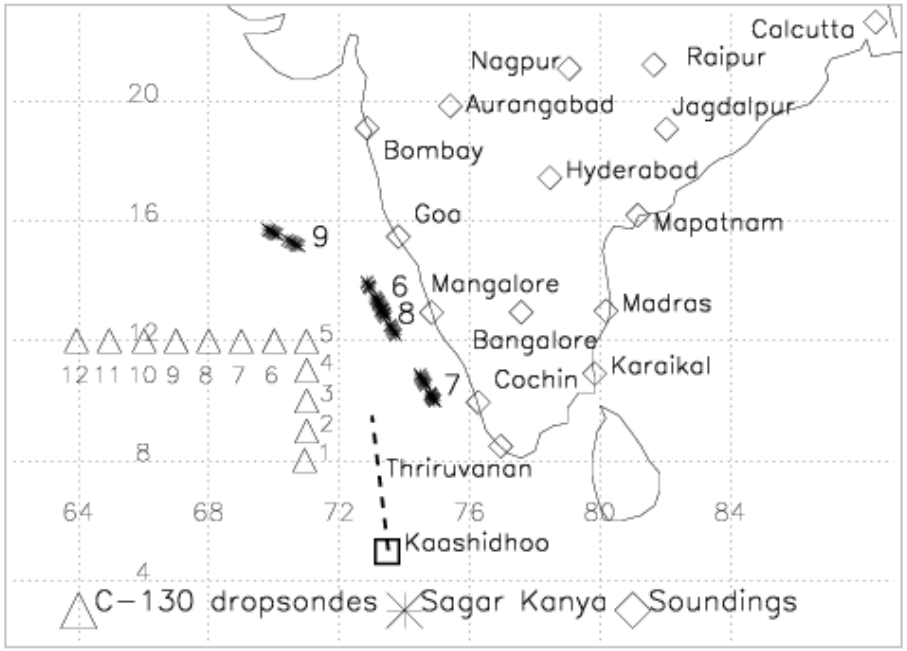

Fig. 1. Location of the sounding stations network over continental India (lozenges), as well as Kaashidhoo, Maldives (square). The Mystère 20 flight track, along which LIDAR data shown in Fig. 2 were acquired, is shown by the thick dashed line. The position of the dropsondes released from the Met Office C-130 Hercules aircraft on 7 March 1999 over the Arabian Sea are shown as triangles. The position of the Research Vessel Sagar Kanya (R/V SK) between 6 and 9 March 1999 (number corresponding to the day of March) is shown as asterisks.

ACPD
5, 3269–3312, 2005

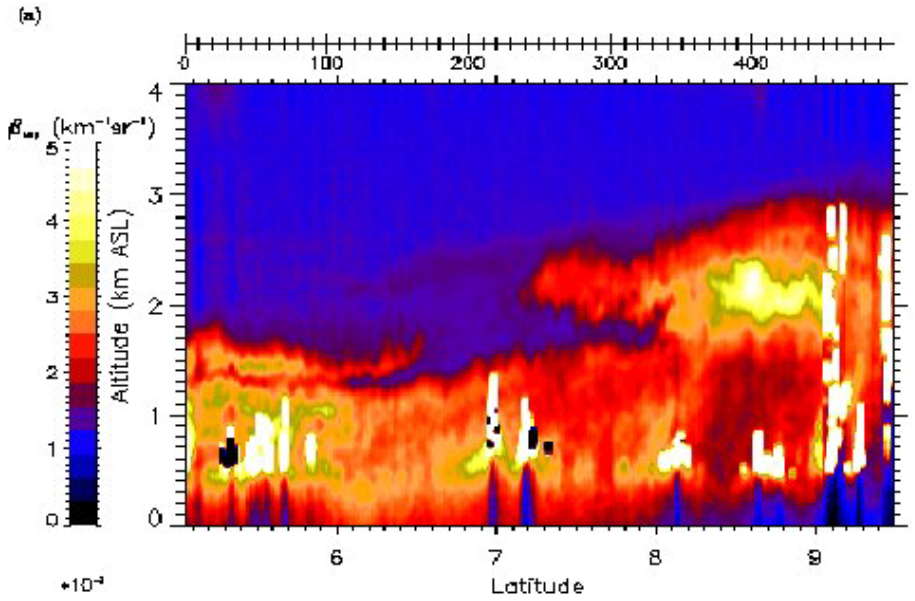

Fig. 2. Attenuated backscatter coefficient obtained at 532 nm by the Leandre 1 Lidar on 7 March 1999 (03:44–04:39 UTC).

ACPD

5, 3269–3312, 2005

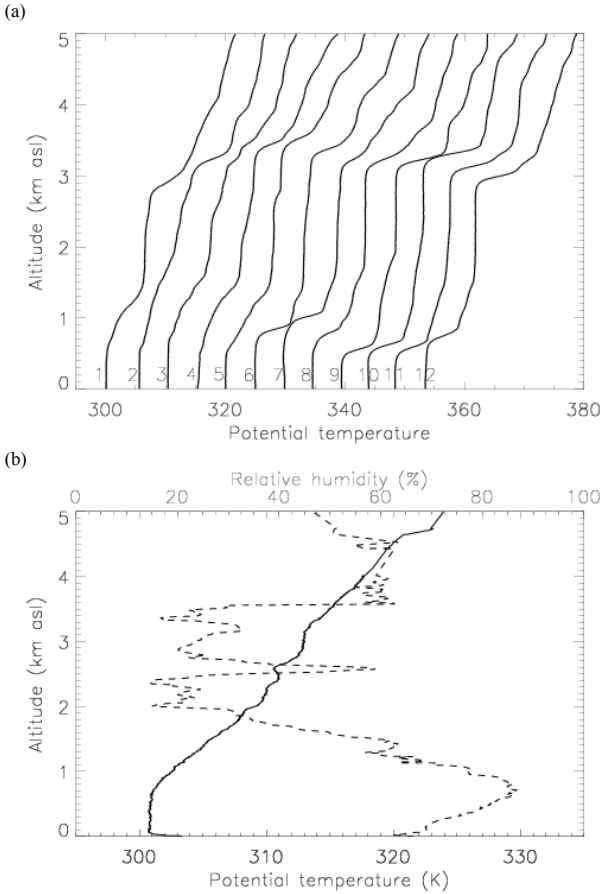

Fig. 3. **(a)** Potential temperature profiles obtained from dropsondes released from the Met Office C-130 Hercules aircraft on 7 March 1999 over the Arabian Sea between 05:19 and 07:34 UTC. **(b)** Potential temperature (solid line) and relative humidity (dotted line) profiles obtained with the 06:11 UTC balloon sounding launched in Kaashidhoo, Maldives.

ACPD
5, 3269–3312, 2005

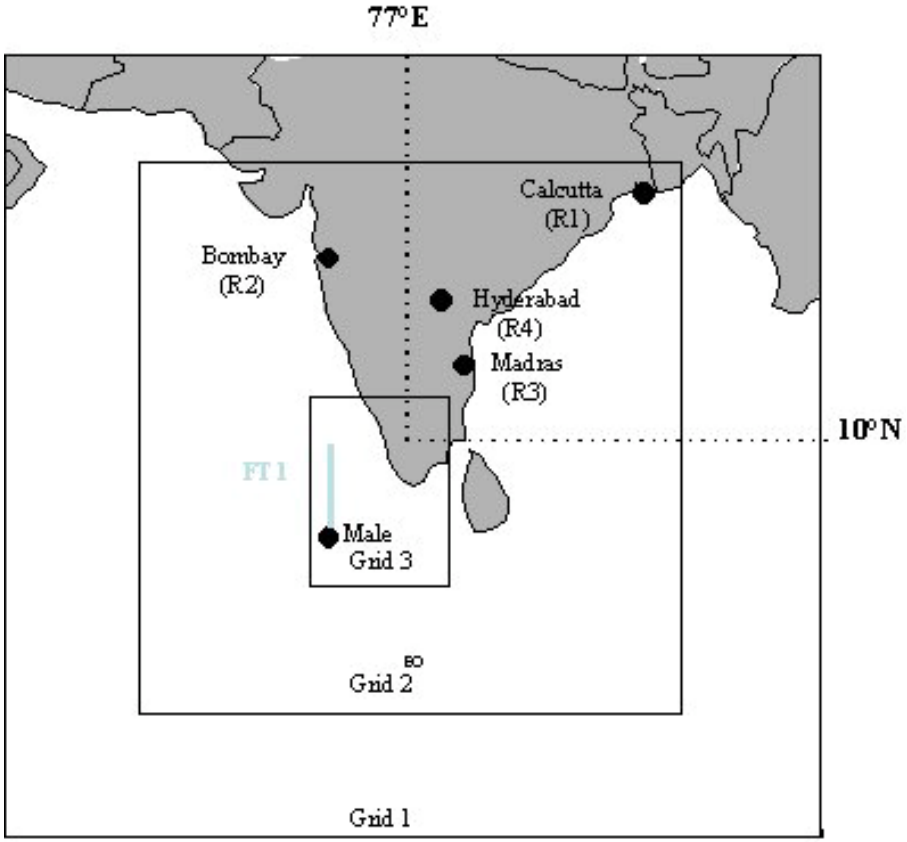

Fig. 4. Simulation domain with position of the 3 nested grids and the 4 emission areas. Calcutta (R1), Bombay (R2), Madras (R3), Hyderabad (R4).

ACPD
5, 3269–3312, 2005

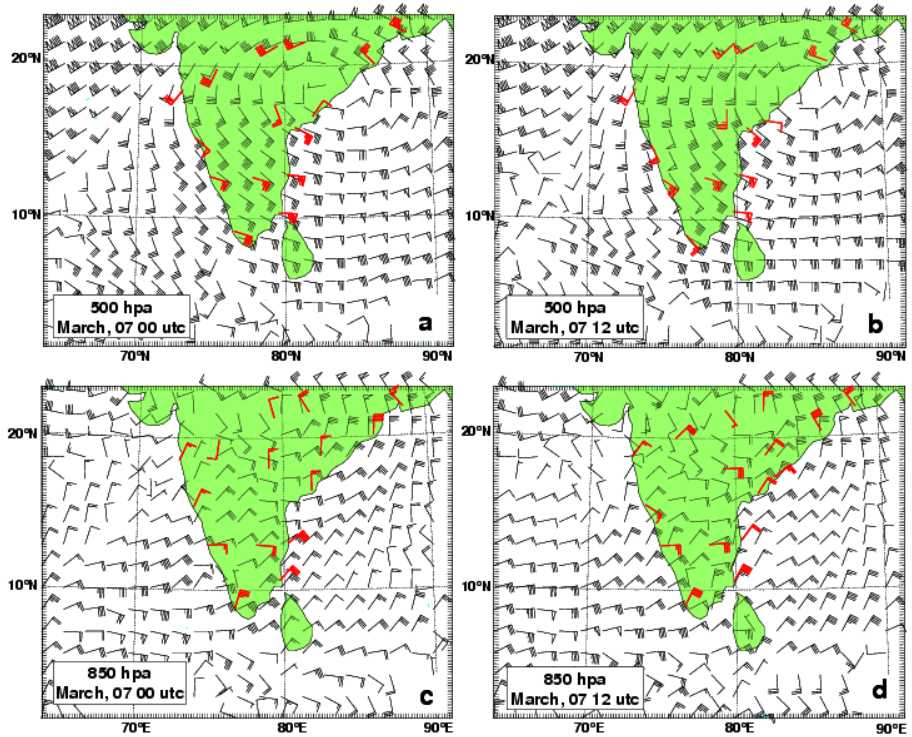

Fig. 5. Horizontal wind fields (black wind barbs) simulated on the intermediate domain (grid 2) at 00:00 UTC for the 500 hPa **(a)** and 850 hPa **(c)** levels on 7 March. Also shown are the wind fields at 12:00 UTC for the 500 hPa **(b)** and 850 hPa **(d)** levels on 7 March 1999. Also shown are the wind barbs extracted at the 500 and 850 hPa levels from the upper air soundings of the Indian network (see Fig. 1 for locations) when available (red wind barbs). Long (short) ticks associated to the wind barbs correspond to 2 m s^{-1} (1 m s^{-1}) ,while triangles correspond to 10 m s^{-1}.

ACPD
5, 3269–3312, 2005

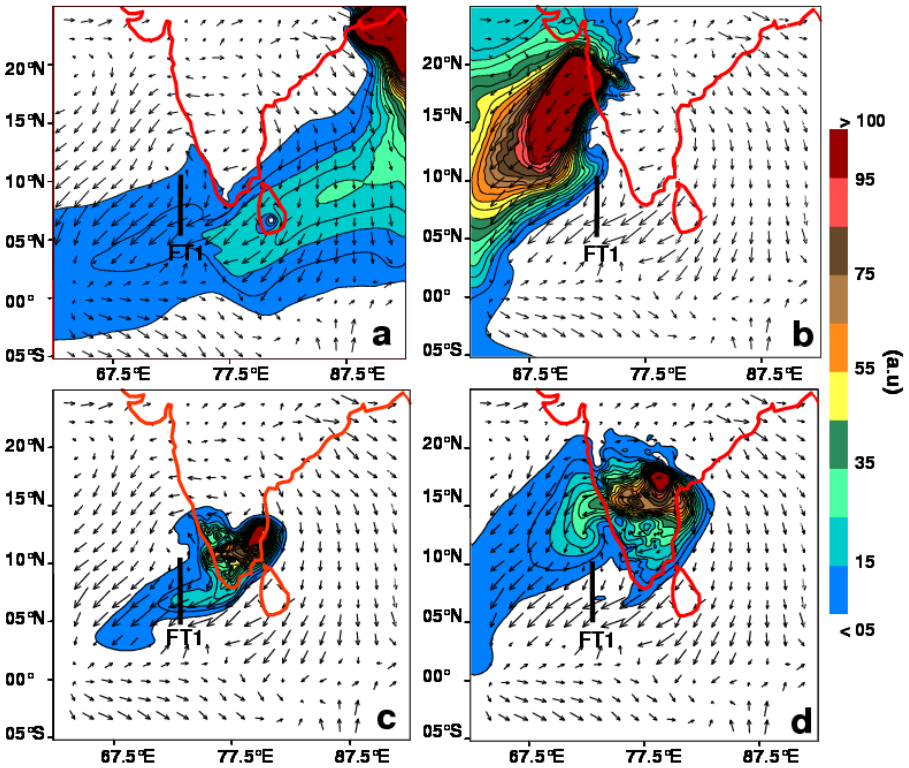

Fig. 6. Horizontal distribution of tracer concentrations (a.u.) at 100 m m.s.l. on 7 March 1999 at 03:00 UTC associated with sources located in **(a)** Calcutta, **(b)** Bombay, **(c)** Madras, and **(d)** Hyderabad for the reference simulation (run B) on grid 2.

ACPD
5, 3269–3312, 2005

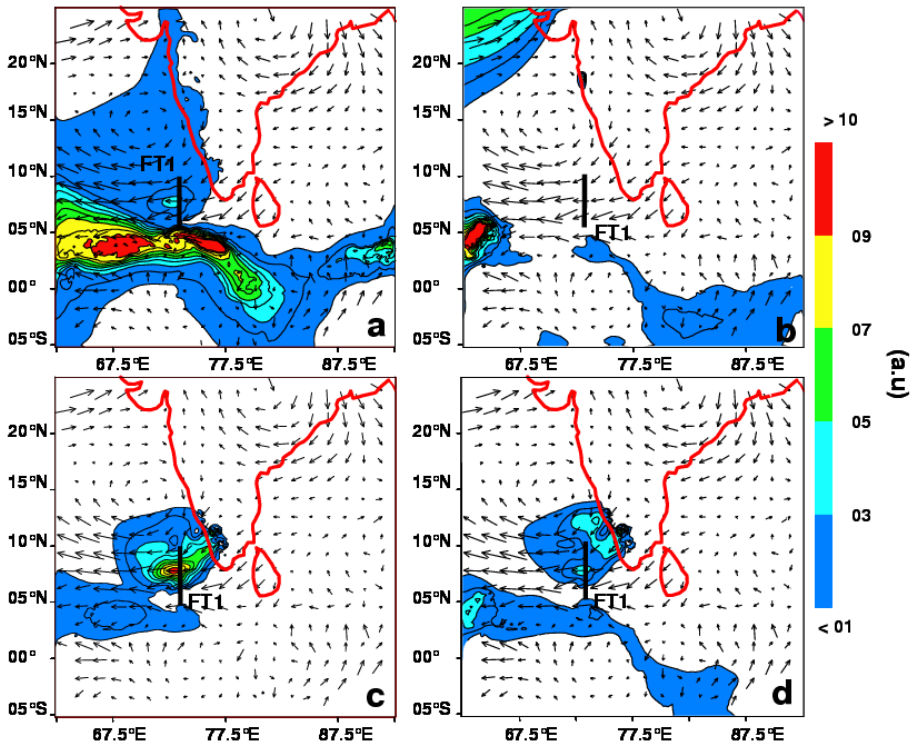

Fig. 7. Horizontal distribution of tracer concentrations (a.u.) at 2000 m m.s.l. on 7 March 1999 at 03:00 UTC associated with sources located in **(a)** Calcutta, **(b)** Bombay, **(c)** Madras, and **(d)** Hyderabad for the reference simulation (run B) on grid 2.

ACPD
5, 3269–3312, 2005

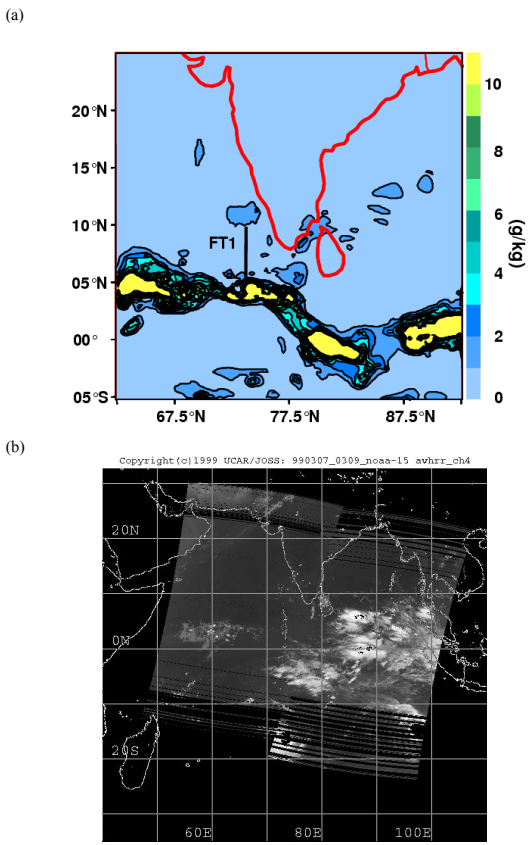

Fig. 8. **(a)** Horizontal distribution of liquid water mixing ratio (g/kg) vertically integrated from ground to top on 7 March 1999 at 03:00 for the reference simulation (run B) in grid 2. **(b)** NOAA 15 infrared image over the Indian Ocean at 03:09 UTC on 7 March 1999. Tropical cyclone Davina is located at 16° S, 75.5° E and the subsequent tropical depression near 15° S, 93° E.

ACPD
5, 3269–3312, 2005

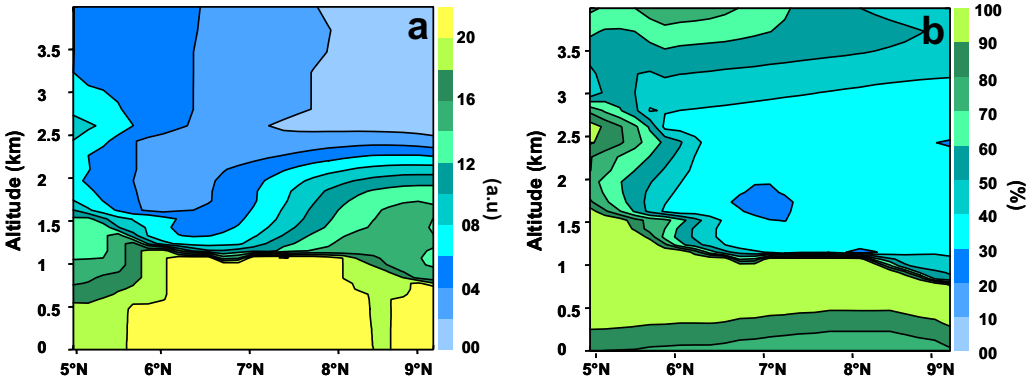

Fig. 9. Vertical distribution of the tracer concentration **(a)** and relative humidity **(b)** along FT1 obtained with the reference simulation (run B) in grid 2 at 03:00 UTC on 7 March 1999. The tracer field in (a) is the sum of the tracer fields from the four emission sources.

ACPD
5, 3269–3312, 2005

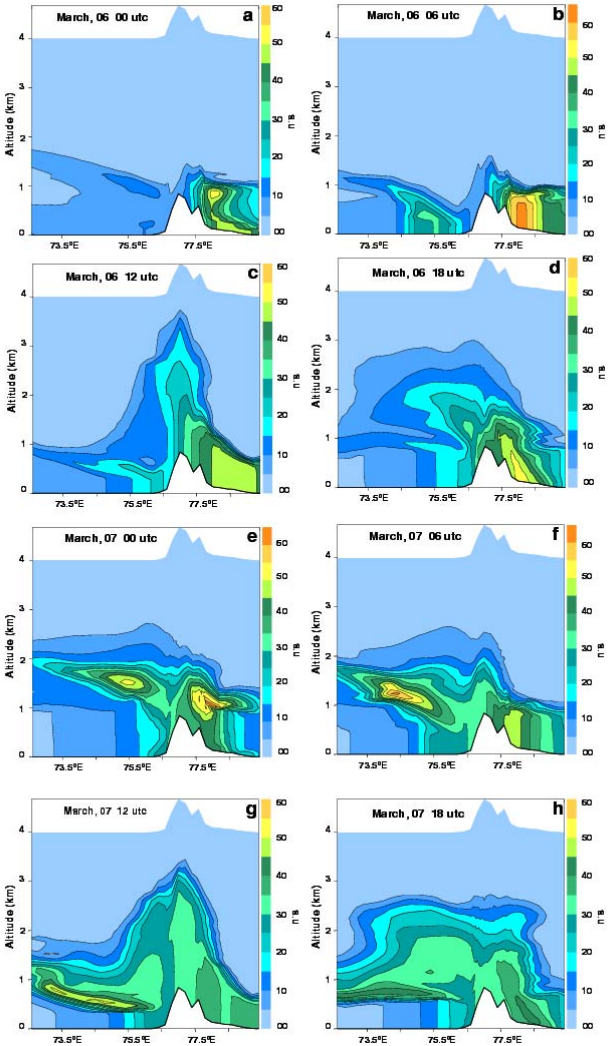

Fig. 10. Vertical distribution of the tracer concentration (u.a.) at 10° N latitude and between 73° E and 78.5° E, obtained with the 2-grid reference simulation (run B) at **(a)** 00:00, **(b)** 06:00, **(c)** 12:00, **(d)** 18:00 UTC on 6 March and at **(e)** 00:00, **(b)** 06:00, **(c)** 12:00, **(d)** 18:00 UTC on 7 March 1999.

ACPD
5, 3269–3312, 2005

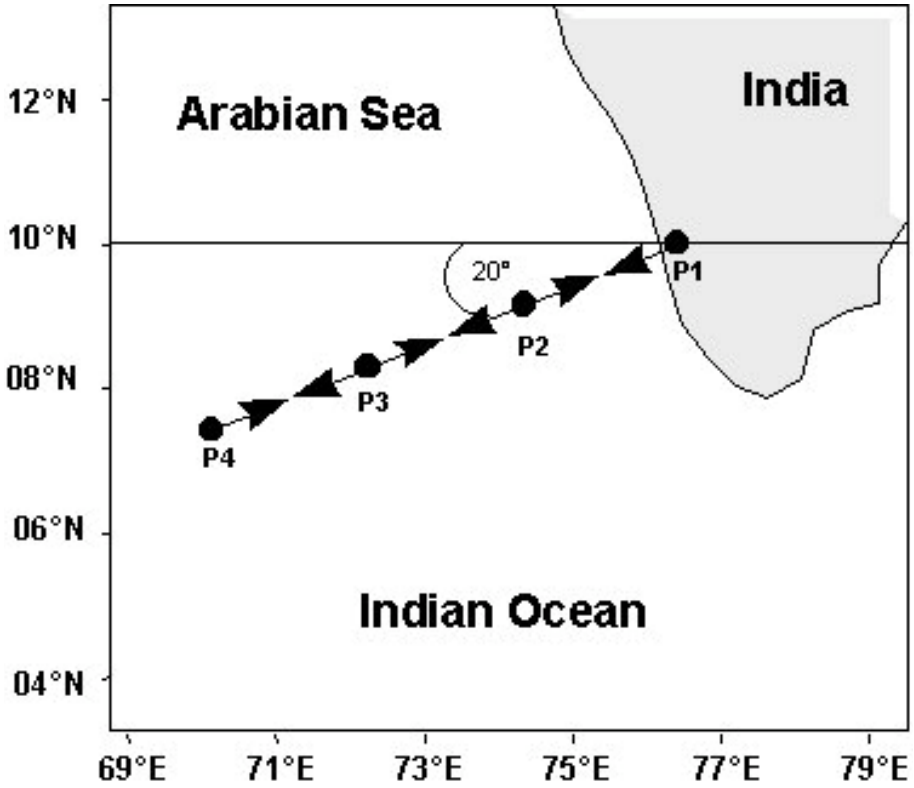

Fig. 11. Map of south India and position of the 4 locations used to inspect the spatial and temporal structure of pollutants plume over the Ocean: P1 (76.5° E; 10° N), P2 (74.3° E; 9.3° N), P3 (72.7° E; 8.6° N), P4 (69.9° E; 7.6° N).

ACPD
5, 3269–3312, 2005

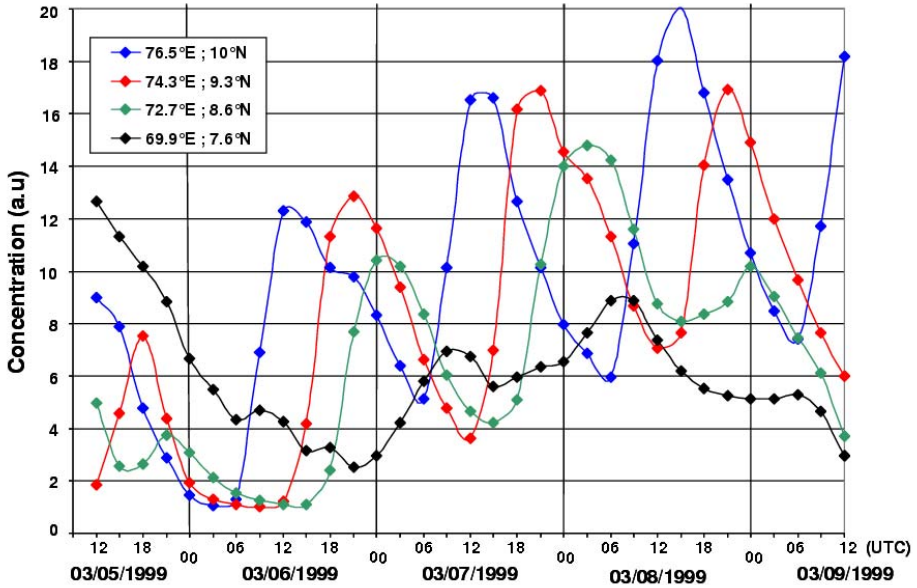

Fig. 12. Diurnal evolution of the top of the tracer plume (2000 meters in altitude) between 5 March (12:00 UTC) and 9 March (12:00 UTC), along mean winds line for (P1, blue), (P2, red), (P3, green) and (P4, black) from the high resolution simulation (run C) in grid 2.

ACPD
5, 3269–3312, 2005

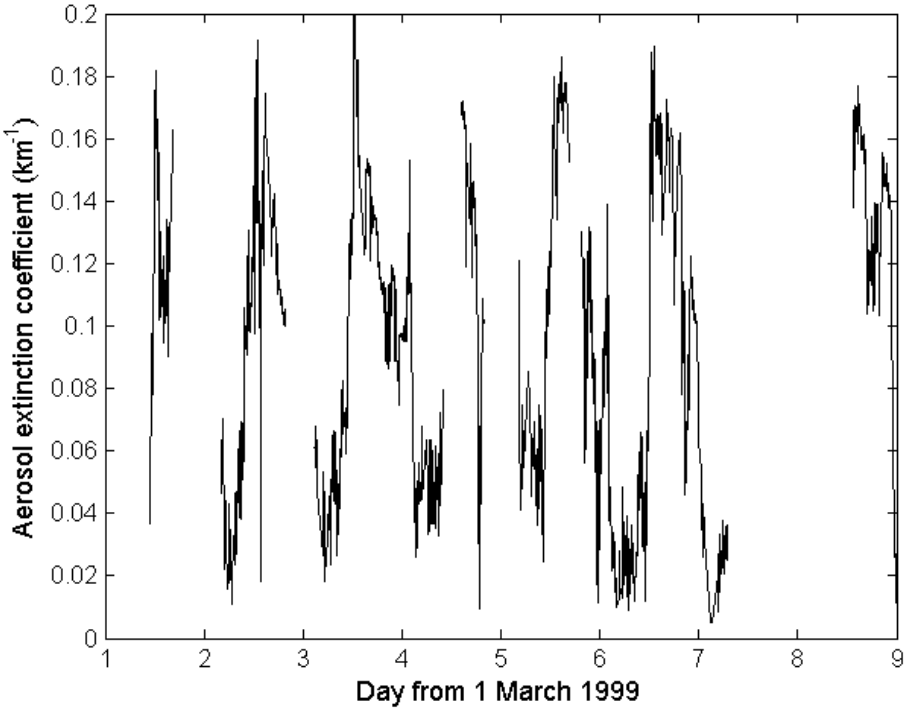

Fig. 13. LIDAR extinction coefficient (at 532 nm) measured in Goa at 2000 m m.s.l. between 1 and 8 March 1999.

ACPD
5, 3269–3312, 2005

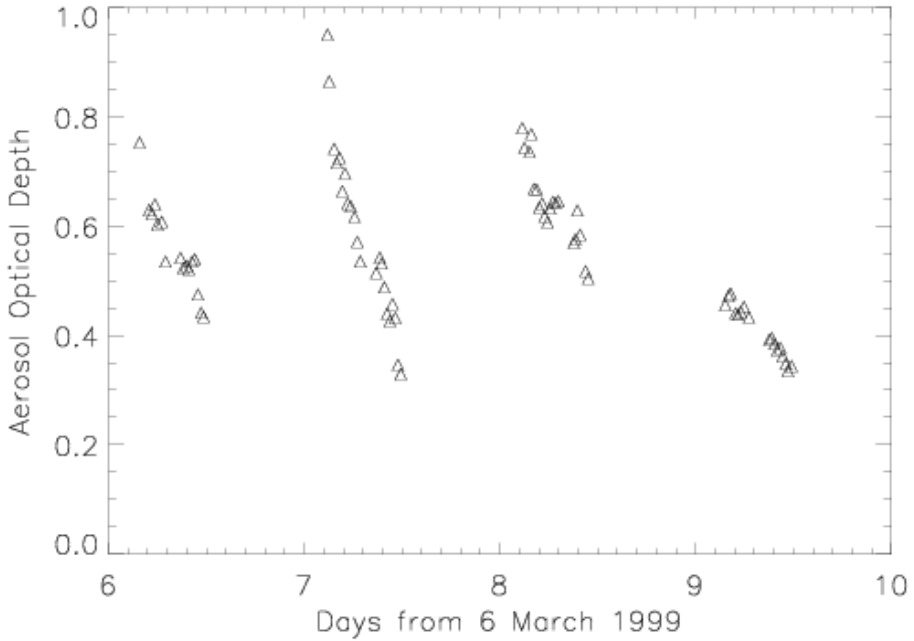

Fig. 14. Sun-photometer aerosol optical depth (at 497 nm) measured onboard the R/V SK between 6 and 10 March 1999. The position at which the measurements were made are shown in Fig. 1.

ACPD
5, 3269–3312, 2005

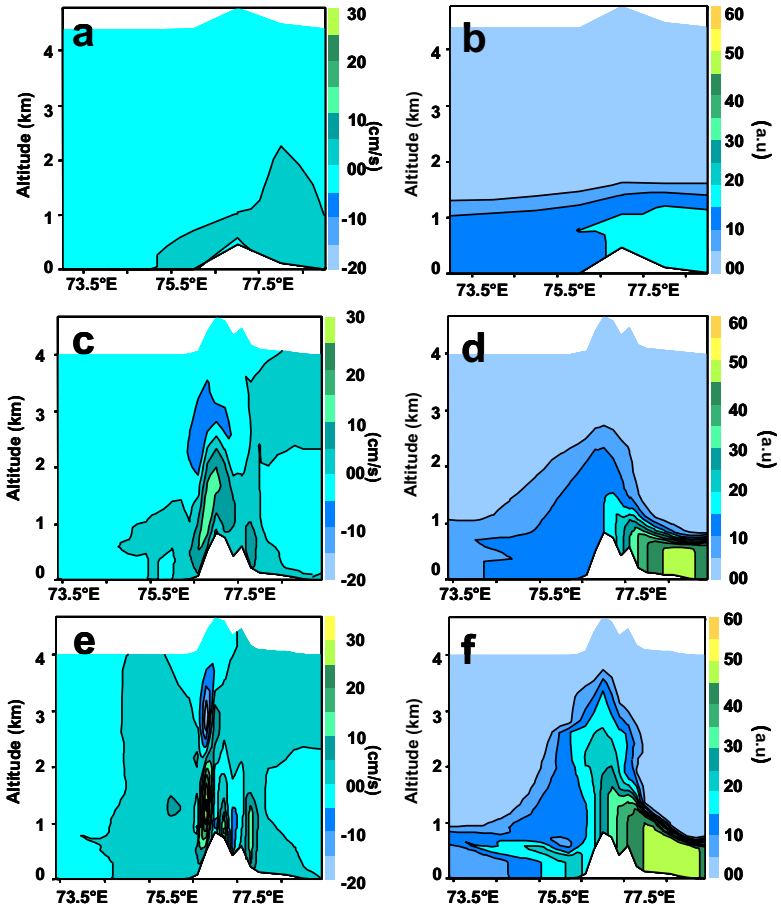

Fig. 15. Vertical distribution of the tracer concentration (u.a.) and vertical velocity (cm s^{-1}) at 10° N latitude and between 73° E and 78.5° E, respectively, obtained with the 1-grid simulation (runA) referred as S1 **(a)** and **(b)**, with the 2-grids reference simulation (run B) referred as S2 **(c)** and **(d)** and with the high resolution simulation (run C) referred as S3 **(e)** and **(f)** at 12:00 UTC on 7 March 1999.

ACPD
5, 3269–3312, 2005

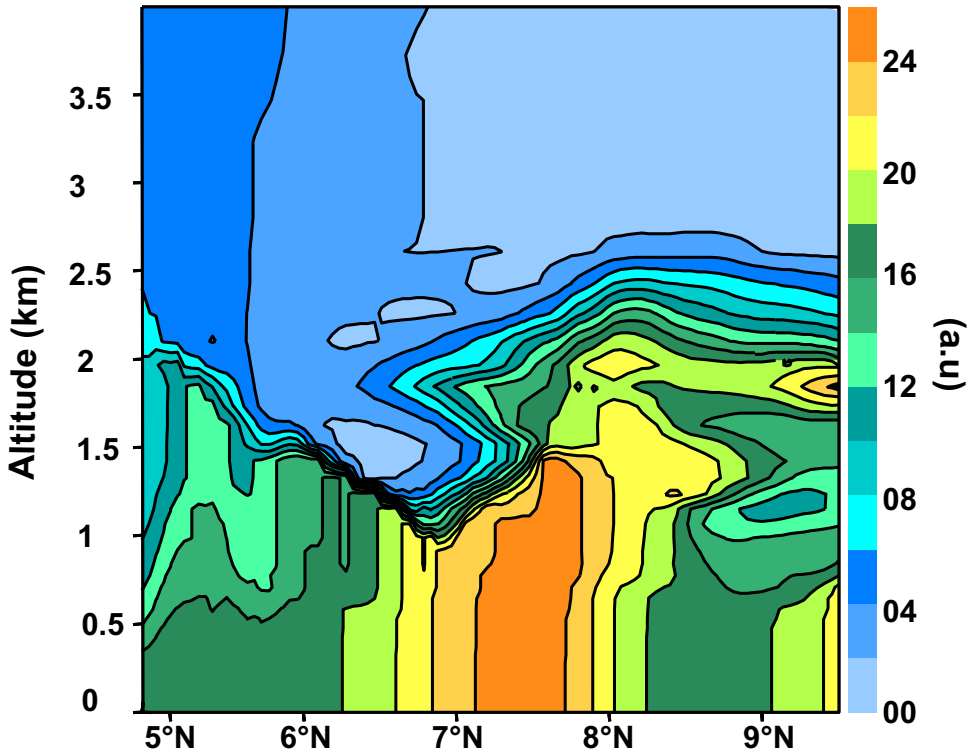

Fig. 16. Vertical distribution of the tracer concentration (all sources) along FT1 obtained with the high resolution simulation in grid 3 (run C) at 03:00 UTC on 7 March 1999. The contours are obtained by summing the tracer fields from the four emission sources.

ACPD
5, 3269–3312, 2005